JNeurosci
THE JOURNAL OF NEUROSCIENCE

Research Articles: Systems/Circuits

Sequential neural activity in primary motor cortex during sleep

Wei Xu, Felipe de Carvalho and Andrew Jackson

Institute of Neuroscience, Newcastle University, Newcastle NE2 4HH, UK

https://doi.org/10.1523/JNEUROSCI.1408-18.2019

Received: 4 June 2018

Revised: 29 January 2019

Accepted: 2 February 2019

Published: 6 March 2019

Author contributions: W.X., F.D.C., and A.J. performed research; W.X., F.D.C., and A.J. analyzed data; W.X. and F.D.C. wrote the first draft of the paper; W.X., F.D.C., and A.J. edited the paper; W.X., F.D.C., and A.J. wrote the paper; F.D.C. and A.J. designed research.

Conflict of Interest: The authors declare no competing financial interests.

We thank Jennifer Tulip for assistance with experiments, Norman Charlton for technical support and Stephanie Lee for performing manual sleep scoring. This work was supported by the Wellcome Trust (106149) and the Engineering and Physical Sciences Research Council (H051570).

Correspondence should be addressed to Andrew Jackson, Institute of Neuroscience, Medical School, Newcastle University, Framlington Place, Newcastle Upon Tyne, NE2 4HH, UK. E-mail: andrew.jackson@newcastle.ac.uk

Cite as: J. Neurosci 2019; 10.1523/JNEUROSCI.1408-18.2019

Sequential neural activity in primary motor cortex during sleep

Wei Xu*, Felipe de Carvalho*, Andrew Jackson

Institute of Neuroscience, Newcastle University, Newcastle NE2 4HH, UK

* These authors contributed equally to this work

Submitting author: Felipe de Carvalho

Correspondence should be addressed to Andrew Jackson, Institute of Neuroscience, Medical School, Newcastle University, Framlington Place, Newcastle Upon Tyne, NE2 4HH, UK.

E-mail: andrew.jackson@newcastle.ac.uk.

Number of text pages:

Number of figures:

Number of words: Abstract (216), Introduction (436), Discussion (1269).

Conflict of interest: The authors declare no competing financial interests.

Acknowledgements: We thank Jennifer Tulip for assistance with experiments, Norman Charlton for technical support and Stephanie Lee for performing manual sleep scoring. This work was supported by the Wellcome Trust (106149) and the Engineering and Physical Sciences Research Council (H051570).

Abstract

Sequential firing of neurons during sleep is thought to play a role in the consolidation of learning, but direct evidence for such sequence replay is limited to only a few brain areas and sleep states mainly in rodents. Using a custom-designed wearable neural data logger and chronically implanted electrodes, we made long-term recordings of neural activity in the primary motor cortex of 2 female non-human primates during free behavior and natural sleep. We used the local field potential (LFP) spectrogram to characterize sleep cycles, and examined firing rates, correlations and sequential firing of neurons at different frequency bands through the cycle. Slow-wave sleep (SWS) was characterized by low neural firing rates and high synchrony reflecting slow oscillations between cortical down and up states. However, the order in which neurons entered up states was similar to the sequence of neural activity observed at low frequencies during waking behavior. In addition, we found evidence for brief bursts of theta oscillation, associated with non-SWS states during which neurons fired in strikingly regular sequential order phase-locked to the LFP. Theta sequences were preserved between waking and sleep, but appeared not to resemble the order of neural activity observed at lower frequencies. The sequential firing of neurons during slow oscillations and theta bursts may contribute to the consolidation of procedural memories during sleep.

Significance Statement

Replay of sequential neural activity during sleep is believed to support consolidation of daytime learning. Despite a wealth of studies investigating sequential replay in association

with episodic and spatial memory, it is unknown whether similar sequences occur in motor areas during sleep. Within long-term neural recordings from monkey motor cortex we found two distinct patterns of sequential activity during different phases of the natural sleep cycle. Slow-wave sleep was associated with delta-band sequences that resembled low-frequency activity during movement, while occasional brief bursts of theta oscillation were associated with a different order of sequential firing. Our results are the first report of sequential sleep replay in the motor cortex, which may play an important role in consolidation of procedural learning.

Introduction

Brain activity during sleep is implicated in stabilizing, consolidating and reorganizing daytime learning, but the neural mechanisms remain unclear. One influential theory is that the reactivation of specific sequences of neural firing observed during the day (sleep 'replay') drives synaptic changes through spike-timing dependent plasticity which depends critically on the temporal order of pre- and post-synaptic activity (Kruskal et al., 2013). Sequential replay was first reported in the hippocampus of sleeping rats (Wilson and McNaughton, 1994), and has since been observed the striatum (Pennartz et al., 2004) and prefrontal cortex (Euston et al., 2007, Peyrache et al., 2009) leading to a wealth of literature concerning the consolidation of spatial and rule learning. However, while sleep is also implicated in consolidation and off-line gains following motor learning (Walker et al., 2002, Nitsche et al., 2010, Tucker et al., 2017), there has been considerably less investigation of single-unit activity in motor areas during sleep. Synchronous reactivation in rodent slow-wave sleep has been linked to consolidation of forelimb reaching behaviors (Ramanathan et al., 2015) but there have been no reports of sequential firing similar to that observed in the episodic memory system. Previously we have shown in monkeys that delta oscillations in local field potentials (LFPs) during anesthesia and slow-wave sleep share a common

structure with 2-3 Hz cortical cycles during awake movements (Hall et al., 2014a). Since neural firing rates exhibit consistent cyclical structure at these frequencies across different awake behaviors (Churchland et al., 2012, Russo et al., 2018), we speculated that the same sequences might also occur at delta frequencies during cortical cycles in slow-wave sleep. In addition, we sought evidence for sequential activity at other frequencies during other phases of the natural sleep cycle.

We used a wearable data-logger to record long-term multichannel spiking activity in the motor cortex of monkeys during free behavior and natural sleep, in order to examine patterns of neural correlation across the sleep cycle. During slow-wave sleep, the dominant pattern was broad synchrony between neurons reflecting the slow oscillation between cortical down and up states. However, neurons entered the up state at slightly different times, leading to sequential activation at low frequencies. This order resembled that seen during awake behavior, suggesting the same intrinsic dynamics governs both states. Outside of slow-wave sleep, and occasionally in awake states, we observed brief epochs of theta oscillation during which neurons fired rhythmically in consistent sequences. Interestingly the order of neural firing during theta bursts was unrelated to that seen at lower frequencies, and we suggest that this represents a different network state that may be well-suited to drive neuroplasticity of motor cortical circuits.

Materials and Methods

Wearable neural data logger

To record long-term neural activity during wake and sleep in non-human primates without the constraints imposed by physical tethers or the limited transmission ranges and battery lifetimes associated with wireless telemetry, we developed a custom wearable neural data logger (Fig. 1). The device incorporated two multichannel bio-amplifiers (gain x192, RHD2132, INTAN Technologies, CA, US) configured to record 8 channels of wideband

neural signals (0.1Hz -7.5kHz bandwidth, 20 kHz sampling rate) and 32 channels of LFP signals (0.1Hz – 300Hz bandwidth, 1 kHz sampling rate). The 16-bit digitized samples were sent via a serial peripheral interface (SPI) to a low-power microcontroller (STM32F407, STMicroelectronics, Geneva, Switzerland) which packaged and relayed the data in time-stamped 16KB blocks to a 64GB microSD card.

The neural logger was implemented on three PCBs (1 x digital board and 2 x headstages, 30x30 mm and 30x20 mm, respectively) which were mounted inside a titanium head casing also containing a 3.7V 5200mAh rechargeable battery. This system was capable of recording for over 24hrs, thereby providing continuous monitoring of neural data with only a daily replacement of the microSD card and battery.

Surgical procedures

Experiments were approved by local ethics committee and performed under appropriate UK Home Office licenses in accordance with the Animals (Scientific Procedures) Act 1986. Two purpose-bred female rhesus macaques (O: 9 y/o, 6.8 kg and U: 6 y/o, 7.2kg) were used for this study. Surgeries were performed in sterile conditions under sevoflurane anesthesia with appropriate post-operative analgesics and antibiotics. The animals were implanted with custom arrays comprising 12 moveable 50µm-diameter tungsten microwires (impedance ~200 kΩ at 1 kHz) and four 16-channel linear microelectrode arrays (LMA, Microprobe). Our moveable microwire array has been described in detail previously (Jackson and Fetz, 2007) and allows electrodes to be individually positioned. We find that these arrays yield stable recordings of the same single units over multiple days to several months. The LMAs were incorporated to provide depth-profiles of local field potentials, and comprised 16 evenly-spaced contacts (separation: 250µm for short LMAs, 500µm for long LMAs). Monkey O received two such combined arrays, implanted bilaterally in the primary motor cortex (M1).

Monkey U received a single array implanted in right M1. Implantation was guided by a prior structural MRI scan and intraoperative identification of the central sulcus.

Additionally, monkey U was implanted with electromyogram (EMG) electrodes in 6 left arm muscles (ECR, ECU, FCR, FCU, Bic,Tri), comprising pairs of insulated stainless steel wire (AS632, Cooner Inc.) sutured to the muscle fascia and routed subcutaneously to the head-mounted titanium casing that contained connectors, electronics and battery.

Home-cage recordings

Overnight recordings were taken following conventional recording sessions in the laboratory, 4 days per week, over a period of 5 months. Here we report only data from recordings that captured a full night of sleep and were not corrupted by excess noise (large artefacts or line noise associated with broken connections). Recordings usually began in the late afternoon and lasted on average 20.9 hrs ± 3.8 hrs (46 nights for monkey O) and 20.4 hrs ± 2.3 hrs (99 nights for monkey U). Variations in the recording period are accounted by different lengths of laboratory sessions and different start times for those sessions.

Spike sorting and spike discrimination

All analyses were performed in Matlab (Mathworks Inc.). Data were initially decoded and saved to a computer using custom scripts. Spike discrimination was performed offline using Wave_clus (Quiroga et al., 2004), configured with a 1-8 kHz bandpass filter and an amplitude threshold of 4 standard deviations (SD) above signal mean for spike detection. From the 12 microwire electrodes we were able routinely to discriminate several single and multi-unit spikes per recording session (example spike waveforms and inter-spike interval (ISI) histograms are shown in Fig. 2E). Analysis is based only on single units exhibiting a clear peak in the inter-spike interval (ISI) histogram and we obtained 0 to 7 such units per

session. For monkey O we recorded 70 M1 single units and for monkey U we recorded 184 single units.

Experimental Design and Statistical Analysis

Assessing stability of spike waveforms:

To verify that the Neurochip was able to record the same neurons throughout these long sessions, we assessed the similarity between the average waveforms of the first 1000 spikes and last 1000 spikes within each session using a coefficient of determination (CoD):

$$CoD = 1 - \frac{\sum_t (s_1(t) - s_2(t))^2}{\sum_t (s_1(t) - \overline{s_1})^2} \quad \text{Eq. 1}$$

where $s_1(t)$ and $s_2(t)$ are the mean waveforms at the start and end of the session, and $\overline{s_1}$ is the mean value of $s_1(t)$. Note that a CoD close to 1 indicates a similar waveform, suggesting that same neuron has been maintained throughout. To compare our experimental CoD values against what would be expected if the neurons were not the same at the beginning and end of recordings, we bootstrapped the distribution of CoD values obtained by comparing spike waveforms recorded at beginning of sessions with spike waveforms for a different neuron at the end of recordings. We performed 1000 iterations of this shuffling procedure in order to test the overall significance of our mean CoD value.

Defining sleep periods:

Data were down-sampled to 250 Hz prior to performing a Fast Fourier Transform (FFT) using a 512-point (2.048 s) window. We defined sleep periods based on the onset and off-

171 set of high amplitude LFP activity averaged over 5 min windows (assessed by eye from
172 power spectrograms – example in Fig. 2A), and validated these judgements in monkey O
173 with simultaneously acquired video recordings. The times of falling asleep and waking up
174 judged from electrophysiological and video recordings were not statistically different (paired
175 t-test, $p = 0.57$ and 0.91 for sleep onset and offset respectively, $n = 22$).

176

177 Defining sleep cycle phase:

178 Conventionally, human sleep periods have been separated into different phases by visual
179 examination of the EEG (Berry et al., 2015). Different sleep phases are associated with
180 relative increases or decreases in power at different frequency bands of the EEG and/or LFP
181 (Iber et al., 2007, Destexhe et al., 1999) but there is no consensus on the number of
182 identifiable discrete sleep states in animals (Kleinlogel, 1990, Gottesmann, 1992). To
183 provide a simple and consistent characterization of the sleep cycle we used the periodic
184 fluctuations in the power of low (<1 Hz) frequency LFPs (Achermann and Borbely, 1997,
185 Steriade et al., 1993b, Steriade et al., 1993a, Destexhe et al., 1999) to derive a continuous
186 measure of sleep phase (Fig. 3A). We low-pass filtered and averaged the low-frequency
187 power in all channels, and applied a Hilbert transform to extract an instantaneous phase that
188 varied from $-\pi$ to π (where zero-phase corresponds to maximal low-frequency power, i.e.
189 slow wave sleep). Sleep phase was divided into ten equal bins for subsequent cycle-aligned
190 analyses of activity patterns.

191

192 Analysis of firing rates through the sleep cycle:

193 The modulation of average firing rates binned by phase through the sleep cycle was
194 assessed using a circular-linear correlation coefficient:

$$r = \sqrt{\frac{r_{xc}^2 + r_{xs}^2 - 2r_{xc}r_{xs}r_{cs}}{1 - r_{cs}^2}} \quad \text{Eq. 2}$$

Where r_{xc}, r_{xs} and r_{cs} are the Pearson's correlation coefficients between respectively: firing rate vs. cosine of sleep phase, firing rate vs. sine of sleep phase, and cosine of sleep phase vs. sine of sleep phase (which equals zero for equally-spaced phase bins). Significance testing was performed using the circ_stats package in Matlab.

Time-domain correlation analyses:

The recording period was divided into consecutive 5 min windows. Within each window we calculated spike-triggered averages (STAs) of LFPs and cross-correlation histograms (CCHs) between simultaneously recorded spike trains (using 10ms-wide bins). CCHs were normalised and expressed as the proportion of excess spike pairs relative to that expected for uniform firing with the same mean rate as the actual neurons within each 5 min window. STAs and CCHs were then averaged over all 5 min windows during wake/sleep periods, or divided according to the phase of sleep that each window occurred within. The strength of spike-LFP correlation was measured as the peak-to-peak amplitude of the STA, while the strength of spike-spike correlation was measured as the zero-lag amplitude of the CCH.

Spike-field coherence:

Spike times were converted into quasi-continuous firing rate signals by binning spikes into 4ms bins, corresponding to the sampling interval of LFPs at 250 Hz. Standard coherence analysis between firing rates and LFPs, $Coh_{spike-LFP}$, was calculated as the magnitude-squared of the normalised complex cross-spectrum, $X_{spike-LFP}$:

$$X_{spike-LFP}(f) = \frac{\sum F_{spike}(f).F^{*}_{LFP}(f)}{\sqrt{\sum |F_{spike}(f)|^2 \sum |F_{LFP}(f)|^2}}$$

$$Coh_{spike-LFP}(f) = \left|X_{spike-LFP}(f)\right|^2 \quad \text{Eq. 3}$$

where $F_{spike}(f)$ and $F_{LFP}(f)$ are the 512-point Fast Fourier Transform (FFT) coefficients of the spike rate and LFP at frequency f, * denotes complex conjugation, and the summation is performed over all windows within a particular interval of the sleep cycle.

Spike-spike coherence:

As with spike-LFP analyses, we also calculated the normalized cross-spectrum between the firing rates of pairs of spikes:

$$X_{spike-spike}(f) = \frac{\sum F_{spike\ 1}(f).F^{*}_{spike\ 2}(f)}{\sqrt{\sum |F_{spike\ 1}(f)|^2 \sum |F_{spike\ 2}(f)|^2}} \quad \text{Eq. 4}$$

The phase of the cross-spectrum reflects the phase difference between neural activity, thus a real value implies in-phase/anti-phase firing whilst a purely imaginary value implies a 90° phase-shift between neurons. It is convenient to decompose the total coherence between spike trains into real and imaginary components:

$$\begin{aligned} Coh_{spike-spike}(f) &= \left|X_{spike-spike}(f)\right|^2 \\ &= \mathrm{Re}(X_{spike-spike}(f))^2 + \mathrm{Im}(X_{spike-spike}(f))^2 \\ &= Coh_{real}(f) + Coh_{imag}(f) \end{aligned} \quad \text{Eq. 5}$$

Note that statistically significant, non-zero imaginary coherence, $Coh_{imag}(f)$, implies that there is a consistent phase order to neural firing at frequency f, although that phase difference not need to be exactly 90°. Non-parametric significance testing of imaginary coherence was carried by bootstrapping the expected distribution of imaginary coherence between neurons in the absence of a consistent phase order between them. To achieve this we used the same Fourier amplitudes as the real data but randomly shuffled the phases of Fourier coefficients across neurons, on a window-by-window basis. We repeated this processes 1000 times and calculated the 95th percentile value of the resultant distribution.

Sequence similarity:

The sign of the (unsquared) imaginary component of coherence, $\mathrm{Im}(X_{spike-spike}(f))$, reflects the order of sequential firing between neurons. This allows comparison of the sequence structure between different behavioral states (e.g. wake vs. sleep). A conserved sequence (e.g. 1->2->3) would be one in which the imaginary coherence between all neuron pairs ([1,2], [2,1], [1,3], [3,1], [2,3], [3,2]) would have the same sign (+,-,+,-,+,- respectively) in both behavioral states. Therefore, we used correlation analysis over all neuron pairs between the different states as a measure of sequence preservation. Note that the imaginary coherence between different pairs of neurons within the same recording cannot be treated as independent observations (trivially, for sessions with two neurons $Coh_{imag}[1,2] = -Coh_{imag}[2,1]$, while the number of pair-wise values grows combinatorially as the number of independent neurons increases). Therefore we used a non-parametric approach to significance testing, based on bootstrapping the expected distribution of correlation values after shuffling the labelling of neurons (not neuron pairs) within the dataset corresponding to one of the behavioral states. Shuffling was performed within each recording session, and across sessions that contained the same number of neuron pairs. In this way we were able to bootstrap the expected range of correlation values from 1000

surrogate datasets of pairwise imaginary coherence values with the same statistical distribution as the original data but no systematic relationship between behavioral conditions.

Results

Continuous long-term recording during waking and sleep

Our wearable neural data logger (Figure 1) provided stable, long-term recordings from multiple motor cortical electrodes in unrestrained monkeys. Figure 2A,B shows example LFP data from a single electrode collected over a 22-hour recording period including awake home-cage behavior and natural sleep. At expanded time resolution (Fig. 2C) spiking activity is evident on top of the LFP, and this is revealed more clearly after high-pass filtering (>1 kHz; Fig. 2D). Example waveforms and inter-spike interval histograms for all single- and multi-unit activity captured in this recording session are shown in Fig. 2E.

To ensure we were recording the same individual neurons across such long sessions, we assessed the similarity between average spike waveforms at the beginning and end of recordings (Fig. 2F, *left*) using a Coefficient of Determination (CoD). Values close to 1 indicate that we were able to maintain highly stability recordings (Fig. 2F, *right*). To ensure that these high CoD values were not simply the result of general features shared by all neurons, we calculated the distribution of CoDs between waveforms of different neurons in our dataset. CoDs for the same neuron at the beginning/end of recordings were significantly greater than CoDs between different neurons ($P<0.001$ for both animals).

LFP oscillations across the sleep cycle

Evident in the LFP time-frequency spectrogram (Fig. 2A) is a cyclical variation in LFP power during the night, between periods of slow-wave activity and periods of higher frequency

284 oscillation. To characterize these sleep cycles, we used the time-varying low-frequency
285 (<1Hz) power (Fig. 3A) to define an instantaneous phase which varied from –π to π (where
286 zero-phase corresponds to maximal slow-wave activity). The mean (±SE) duration of sleep
287 cycles was 60 ± 3 minutes (monkey O, 46 sessions) and 55 ± 1 minutes (monkey U, 99
288 sessions), consistent with previously reported sleep cycles of 40-60 minutes for macaques
289 (Campbell and Tobler, 1984, Jackson et al., 2007). The mean power <1Hz was significantly
290 lower in the second half of the sleep duration compared to the first (paired t-test, monkey O:
291 P = 0.003, monkey U: P = 2.20e-9), in keeping with a homeostatic decrease in sleep
292 pressure (Vyazovskiy et al., 2007).

293 Figure 3B shows example modulation of power in other LFP bands corresponding to delta
294 (1-4Hz), theta (4-7Hz), alpha (7-15Hz), beta (15-31Hz) and gamma (>31Hz). Using the
295 instantaneous measure of sleep phase derived from <1Hz power, we averaged the
296 modulation of power at other frequencies over the sleep cycle. We normalized power either
297 as a proportion of the average power at that frequency across the sleep cycle (Fig. 3C), or
298 as a proportion of total power across all frequencies for that sleep phase (Fig. 3D). These
299 sleep cycle-averaged power spectrograms revealed clearly the reciprocity between LFP
300 activity at low (<4 Hz) frequencies associated with phases of maximal slow-wave activity,
301 and high (>7 Hz) frequencies during lighter sleep phases. For the theta (4-7Hz) band,
302 absolute power was highest during slow wave phases (Fig. 3C) but this represented a
303 smaller proportion of total power than during lighter sleep (Fig. 3D).

304

305 *Single unit firing rates and EMG activity across the sleep cycle*

306 The firing rates of single neurons also varied during the sleep cycle. For the example neuron
307 shown in Fig. 4A,B, firing decreased during slow-wave sleep (corresponding to sleep phases
308 around 0). Average normalized firing rates across the sleep cycle (using our instantaneous
309 sleep phase measure) revealed this to be the dominant pattern for the majority of neurons

(Fig. 4C). High firing rates observed outside slow-wave sleep are indicative of rapid eye movement (REM) periods, which are characterized by brain activity resembling the waking state but profound paralysis of muscles (Brooks and Peever, 2012, Steriade and McCarley, 1990). For monkey U we were able to obtain simultaneous EMG recordings from 6 muscles in the left forearm during sleep via implanted EMG electrodes as well as simultaneous single unit spiking in the M1 (Fig. 4D). As reported previously (Jackson et al., 2007) periods of high cortical firing rates were often associated with profoundly suppressed EMG (Fig. 4E). We identified putative REM sleep as any 30s periods in which firing rates exceeded average waking levels while average rectified EMG was less than 2μV (Berry et al., 2015). Such windows tended to fall more often around instantaneous sleep phase values of π and –π (Fig. 4F, *top*). Finally, we validated our sleep phase measure by having 300 randomly selected 10s sections of LFP and EMG data from Monkey U scored manually by an experienced EEG sleep technician who was blinded to our results (Fig. 4F, *bottom*). Again, REM sleep was associated with sleep phases of π and –π while sleep phases of zero tended to be scored as stage 2 and 3 of slow-wave sleep. This further supported our use of the instantaneous phase of slow-wave power as a simple yet robust method of characterizing the sleep cycle in non-human primates.

Correlations between spikes and LFPs during wake and sleep

To investigate how the dynamics of the neural population varied across the sleep cycle, we first examined the relationship of single neuron spiking to the LFP. Previously we have shown that spike-triggered average LFPs reveal a low-frequency component (termed the 'spike-related slow potential – SRSP) with a similar shape in both waking and light sleep states (Hall et al., 2014b, Hall et al., 2014a). Note that the biphasic shape may be due to causal filtering by the amplifiers of a monophasic trough (Okun, 2017). SRSPs were also evident in our overnight recordings (Fig. 5A), with a magnitude that varied systematically

through the sleep cycle (Fig. 5B) being largest during slow wave sleep. Spike-field coherence (Fig. 5C) confirmed strong phase-locking at slow oscillation frequencies during slow wave sleep, as well as weaker coherence at alpha frequencies (7-15Hz) during non-slow-wave phases.

Next we examined correlations between pairs of neurons using normalized cross-correlation histograms (Fig. 5D; see Methods). The majority of zero-lag cross-correlations were positive during sleep (100% for monkey O and 97% for monkey U; Fig. 5E) and significantly greater than during waking ($P < 0.05$, paired t-test for both monkeys). Correlated neural firing was also modulated across the sleep cycle, with the highest synchrony occurring during slow-wave sleep (Fig. 5F).

In summary, motor cortical neurons are broadly synchronized during slow-wave sleep, and strongly phase-locked to low-frequency LFP. The shape of the SRSP suggests neurons are maximally active during the negative-going LFP. This likely reflects the known relationship between cortical up/down states (characterized by high/low firing rates respectively) and the slow oscillation observed in the LFP (Steriade et al., 1993b, Steriade et al., 2001). Outside slow-wave sleep neural activity is less synchronized, but weakly phase-locked to LFP activity in the alpha frequency band (7-15Hz) which may correspond to sleep spindles.

Sequential neural firing during slow-wave sleep

Although the dominant pattern of correlation between neurons during sleep was broadly synchronous, we examined whether there was evidence for sequential activity at any frequency. Since spike-triggered averages suggested that neural firing was modulated with the slow LFP oscillation, we first examined the firing rates of multiple neurons aligned to the trough of the low-frequency LFP. The example in Fig. 6A clearly shows an increase in firing rates (the up state) occurring during the falling phase of the slow LFP oscillation. Note

however that this firing rate increase occurs at a slightly different latency for each neuron, leading to a sequential transition into the up state.

A convenient way to quantify such sequential firing in the frequency domain uses the imaginary coherence between pairs of spike trains. Conventional coherence is expressed as the magnitude squared of the (complex) normalized cross-spectrum, but this can be decomposed into the sum-squared of real (in-/anti-phase) component and imaginary (quadrature-phase) components. Non-zero imaginary coherence implies that for a given frequency, the activity of one neuron consistently lags or leads the other (although not necessarily by exactly 90°). Figure 6B shows the decomposition of coherence into real and imaginary squared components for an example spike pair. At very low frequencies, coherence was dominated by a large, real component reflecting correlated in-phase modulation. However, a peak in imaginary coherence around 2-3 Hz revealed consistent sequential activity in the delta band. Note that sequential firing at this frequency was observed during both waking and sleeping states.

We next examined how real and imaginary coherence between neurons was modulated through the sleep cycle (Fig. 6C). Real squared coherence was dominant at low frequencies and was highest during slow wave sleep. Additionally during slow-wave sleep, a statistically significant (albeit weak) imaginary component at delta frequencies was observed, indicating sequential activation through the slow oscillation.

Sequential firing during theta bursts

The previous analysis suggests that when averaged across the entire day or night, sequential firing of neurons (indicated by imaginary squared coherence) is weak and limited to the delta band. However, visual inspection of the raw data revealed occasional distinctive bursts of highly rhythmical theta band oscillations at around 4-5 Hz (two examples in Fig.

386 7A). During these theta bursts, multiple neurons were phase-locked to the oscillation but
387 fired in sequence with different preferred phases.

388 To quantify this phenomenon, we focused our analysis on only 60 time-windows (of length
389 2.048s) from each recording that had the highest relative (proportion of total) LFP power at
390 theta frequencies. Cross-correlation histograms compiled between spike trains for these
391 theta burst windows showed clear oscillatory correlations, with peaks at non-zero time-lags
392 revealing sequential activation (example in Fig. 7B). As before, we used the imaginary
393 coherence between spike trains to assess the consistency of sequence structure within theta
394 bursts. Clear peaks around 4-5 Hz were evident when we restricted our analysis to only the
395 60 time-windows characterized by highest relative theta LFP power (Fig. 7C, *left*). Note that
396 such sequential theta firing was a relatively rare occurrence throughout a single recording.
397 We chose 60 windows because including more windows tended to reduce the strength of
398 imaginary coherence at theta frequencies. When we analyzed a different subset of 60
399 windows, ranked 121-180th in relative theta power, no imaginary coherence was observed
400 (Fig. 7C, *right*). Analysis of windows ranked 61-120th in relative theta power yielded
401 inconsistent results with only small peaks in imaginary coherence in some sessions.

402 Next, we examined whether this sequential firing phenomenon was restricted to the theta
403 band, or if it could be observed during epochs of LFP oscillation at other frequencies.
404 Therefore we repeated our analysis of imaginary coherence using 60 windows selected to
405 have the highest relative LFP power at a range of frequencies up to 20 Hz. The results for
406 one session are shown in the 2D color plot on the *left* of Figure 7D. The vertical axis shows
407 the LFP frequency selected, while the horizontal axis shows the frequency of spike-spike
408 imaginary coherence. The dominant feature is a peak in theta coherence, occurring only
409 when windows are selected for high theta LFP power. As before, this peak disappeared
410 when windows ranked 121-181th in relative LFP power were analyzed (Fig. 7D, *right*). We
411 summarized the entire dataset by plotting the proportion of statistically significant imaginary
412 coherence values in each frequency bin across all sessions for both animals (Fig. 7E; see

Methods). Sequential firing during theta bursts was a consistent finding in the majority of sessions, occurring most commonly during windows selected for high LFP power at 4 Hz. Although theta power during these selected windows was at least 4 times greater than average, firing rates were only slightly higher than other windows at the same sleep phase. Theta bursts predominantly occurred during non-slow wave sleep around sleep phases of ±π (Fig. 7F), consistent with REM and/or light sleep states which in humans are characterized by theta oscillation. Note however that a proportion of theta bursts in both animals also occurred during periods of awake recording (14% for monkey O, 29% for monkey U).

Sequential orders are preserved across sleeping and waking periods

The unsquared imaginary coherence between pairs of spike trains provides an indication of not only the strength (magnitude) but also the order (sign) of sequential firing. This allowed us to examine whether the sequence of firing was preserved at given frequencies between waking and sleep. We first assessed whether any sequential order was preserved between the entire durations of wake and sleep periods. Figure 8A (*top row*) shows example signed imaginary coherence spectra for three cell pairs during waking and sleep. If there were no relationship between sequential firing in wake and sleep, we would expect the sign of imaginary coherence in each state to be unrelated. However the strong resemblance between delta frequency components in each condition (negative, positive, positive respectively for pairs 1, 2 and 3) suggests that if pairs of cells that fire in consistent order during sleep also tend to fire in the same order during waking.

We also calculated signed imaginary coherence spectra for only those 60 windows (in either waking or sleep) which had the highest relative LFP power at theta frequency (Fig. 8A, *bottom row*). In this case a (negative) trough was observed for all three cell pairs in each condition. This again suggests a conserved order of firing between waking and sleep, but

one that is different during theta bursts to that seen at delta frequencies. Note that this difference can also be seen by comparing the examples in Figs. 6A and 7A (*lower plot*) which come from the same session and have the same color-coding of neurons. The order of firing during the up-state (Fig. 6A) differs clearly from the order seen during theta bursts (Fig. 7A, *lower plot*).

To assess the conservation of sequences across the entire dataset, we calculated the correlation between signed imaginary coherence values in wake and sleep periods at each frequency for all cell pairs in both animals (Fig. 8B). Because pairwise coherence values are not statistically independent samples, the significance of these correlation coefficients were tested using shuffling (over neurons rather than neuron pairs; see Methods) to bootstrap 95% confidence interval (grey lines).

Statistically significant similarity between waking and sleeping sequential relationships was observed across the delta band in both animals. The bottom panels of Figure 8B show scatter plots of wake/sleep imaginary coherence between all cell pairs in each animal for an example frequency of 2 Hz.

We also repeated this analysis for the subset of 60 windows in wake and sleep characterized by high LFP theta power (Fig. 8C). In this case, significant sequential similarity between wake and sleep was restricted to only the theta frequency. The bottom panels of Figure 8C show scatter plots of wake/sleep imaginary coherence between all cell pairs in each animal at 4 Hz. Finally, we asked whether the sequence of firing during theta bursts was related to the delta band sequential firing during waking. Figure 8D shows the relationship between 4 Hz imaginary coherence during theta bursts in sleep and 2 Hz imaginary coherence during the entire waking period. It can be seen that these sequential relationships are unrelated, suggesting that delta-band sequential firing and theta bursts reflect different phenomena.

Sequential strength is preserved through first and second halves of the night

We were interested in whether the proportion of theta bursts and/or the strength of sequential activity at either delta or theta frequencies changed systematically through the night. Therefore we divided the night-time recording into two equal halves and compared the average number of high theta windows that fell within each half. In addition we used the average imaginary coherence between neuron pairs as a measure of the strength of sequential activity and compared this between first/second halves of the night in the delta and theta bands, as well as for only high theta windows. We found no significant changes in any of these metrics in either animal (Figure 9) suggesting that sequences occur equally often and equally strongly throughout the night.

Inconsistent sequential spike firing during sleep spindles

Since the LFP during lighter sleep states contained clear spectral peaks at frequencies close to the alpha/sigma band (7-15 Hz) (Figure 3C,D) and neural firing was phase-locked to this rhythm (Figure 5C). We were therefore interested in whether there was evidence for sequential firing associative with these putative sleep spindles. The peak frequency was slightly different in each animal, as revealed by the averaged power spectrum of LFPs in Figure 10A. Therefore in order to isolate epochs mostly likely to contain sleep spindles we selected windows with proportionally high power at these specific frequencies (7.3Hz and 11.7Hz for Monkeys O and U respectively). Figure 10B (*left*) shows an example event recorded from Monkey U, in which a burst of high spindle-frequency LFP is associated with rhythmic firing in three neurons. Cross-correlation histograms for 60 such windows show that these neurons fire in sequence (Figure 10B, *right*). We applied the same approach as previously to select windows associated with high proportional LFP power at a range of frequencies between 7 to 15 Hz. Across all the data in Monkey U, there was a clear peak in imaginary coherence at around 12 Hz when windows with high LFP power at this frequency

were isolated (Fig. 10C). Note however that the magnitude of imaginary coherence substantially lower than at theta frequencies, and statistically significant in only approximately 15% of sessions. In Monkey O we did not observe consistent sequential spiking at any frequency in the spindle range. Figure 10D shows an example spindle event with associated neural firing. In this case the pattern of correlation between neurons was synchronous. Analysis across all sessions revealed no clear or significant imaginary coherence within the spindle band. Therefore we conclude that sequential spiking during sleep spindles is at best a rare and inconsistent phenomenon that varied across animals.

Discussion

Two distinct patterns of sequential firing in motor cortex during sleep

Despite good evidence for a role in sleep rhythms in procedural learning (Nitsche et al., 2010, Walker et al., 2002), there have been few detailed studies on the structure of motor cortical activity during sleep (but see Ramanathan et al. (2015)). Studies in non-human primates have mainly focused on neuronal correlations during awake motor tasks in which the dominant pattern is synchronous discharge in the beta band (Baker et al., 2001, Jackson et al., 2003) and sequential activity at lower frequencies (Churchland et al., 2012), while observations of precise firing sequences (Prut et al., 1998) have subsequently been questioned (Baker and Lemon, 2000). Hoffman and McNaughton (2002) observed sequential reactivation of neural ensembles in monkeys during rest following a maze task but did not study sleep. Our principal aim was therefore to examine correlations between motor cortical neurons at different frequencies across the sleep cycle, and relate these patterns to those seen during waking behavior.

We quantified sequential activity as consistent, non-zero phase relationships between oscillatory firing patterns (measured by imaginary spike-spike coherence), and therefore cannot discount the further presence of non-oscillatory sequences. Nevertheless, using long

517 datasets recorded in monkeys during natural sleep we were able to identify two distinct
518 patterns of sequential activity, at delta and theta frequencies, occurring at different phases of
519 the sleep cycle. These may correspond to “slow” and “fast” modes of oscillatory dynamics
520 that have been observed across multiple memory systems (Headley and Paré, 2017).

521

522 *Delta sequences*

523 During slow-wave sleep, we observed sequential activation in the delta band as neurons
524 entered cortical up states in a conserved order. The sequential order (established by the
525 sign of imaginary coherence between neuron pairs) was significantly similar to that seen at
526 2-3 Hz during awake behavior. The peak in imaginary coherence around 2-3 Hz corresponds
527 to the frequency of movement-related cyclical dynamics observed in 2D projections of the
528 high-dimensional trajectories of neural firing (Churchland et al., 2012) and LFPs (Hall et al.,
529 2014a). Note that imaginary coherence and rotational state-space dynamics are essentially
530 the same phenomenon; state-space rotation implies neurons are consistently active at
531 different phases of a cycle and therefore exhibit imaginary coherence. Conversely, a
532 consistent non-zero phase difference between neurons yields consistently rotating
533 trajectories in state-space projections.

534 Previously we have shown that the phase structure of such cyclical LFP dynamics is
535 conserved between movement and sleep (Hall et al., 2014a). Our present results extend this
536 finding by demonstrating that the sequential structure of single neurons is similarly
537 constrained across waking and slow-wave sleep. The ubiquity and consistency of these
538 cycles further strengthens the hypothesis that low-frequency dynamics do not reflect any
539 particular sensorimotor context but are instead an intrinsic property of motor networks. We
540 suggest that the neural activity associated with specific behaviors is constrained by this
541 sequential structure, which demarcates a manifold of possible patterns within which specific

neural strategies are embedded. It is interesting to note that a similar theory has already been proposed in the sensory domain (Luczak et al., 2009).

Theta sequences

Our second finding was more unexpected, namely that motor cortex neurons fire in strikingly regular sequences during brief bursts of theta band oscillations. These bursts were a rare but robust and statistically significant phenomenon in both animals, clearly evident in the raw recordings.

In rodents, theta oscillations are normally associated with the hippocampus and implicated in spatial navigation and memory (Buzsaki, 2002, Colgin, 2013). Tonic theta oscillations are observed during exploration, and the sequence of place cell firing within the theta cycle is thought to represent the temporal order of experience (Gupta et al., 2012). Theta is rarely investigated in motor areas although a previous study has described sequential activity at theta frequencies in rodent motor cortex during reaching behaviors (Igarashi et al., 2013), possibly reflecting the coupling of hippocampal theta to limb movements (Semba and Komisaruk, 1978). Theta oscillations are also observed in the hippocampus during REM sleep (Colgin, 2013) during which place cells fire in sequences that resemble those seen in awake exploration (Louie and Wilson, 2001). Generally, theta activity is thought to have a role in facilitating communication between areas (Jones and Wilson, 2005) and/or driving plastic changes to network connectivity via spike timing-dependent plasticity (Sadowski et al., 2016).

In humans, theta oscillations comprise shorter, discrete events, and it is thought that multiple independent mechanisms contribute to the generation of these bursts in the hippocampus and cortex (Cantero et al., 2003). Theta is generally investigated in relation to working (Raghavachari et al., 2001) or spatial memory tasks (Kahana et al., 1999, Bush et al., 2017) and not generally associated with motor areas. Nevertheless theta burst stimulation is a

568 reliable way to induce plasticity in the motor cortex (Teo et al., 2011) and some evidence
569 supports a role for REM sleep in the consolidation of procedural memory (Nitsche et al.,
570 2010). Theta oscillations have been observed in prefrontal and anterior cingulate cortices in
571 humans during REM sleep by Vijayan et al. (2017), who suggested role in consolidation of
572 procedural and emotional memories. Such a hypothesis is supported by our present results,
573 which show that cortical theta in non-human primates is associated with sequential neuronal
574 activity similar to that seen in the hippocampus of rodents. The temporal asymmetries up to
575 around 50 ms that we observed in cross-correlation histograms (e.g. Fig. 7B) are within the
576 time-window known to drive known spike timing-dependent plasticity mechanisms *in vivo*
577 (Jackson et al., 2006). Interestingly, the sequences of neural firing observed at theta
578 frequencies bore no resemblance to that seen at lower delta frequencies during waking and
579 sleep. These activity patterns would thus seem to reflect a different network state and one
580 that, speculatively, may have appropriate properties to drive neuroplastic changes in motor
581 networks. We were not able to observe a change in sequential strength from the first to
582 second half of the night. However, further studies involving training on specific behavioral
583 tasks in association with long-term neural recordings may be required to provide evidence
584 for such a role of these theta sequences in neural plasticity motor learning.

585

586 *Advantages of long-term recording with a neural data-logger*

587 Chronic electrode techniques such as our moveable microwire arrays enable the same
588 neurons to be stably monitored long-term, allowing comparison between activity patterns
589 during both waking behavior and natural sleep states. However, for non-human primates in
590 particular, such experiments require a wireless approach to data recording. One method is to
591 use radio-frequency telemetry, but the wide bandwidth of neural data and large transmission
592 distances within home-cages necessitates high power consumption, limiting battery lifetimes
593 to short recording durations (Yin et al., 2014). An alternative solution, as in our present

study, is to record data locally on the implant (Mavoori et al., 2005, Zanos et al., 2011). With the growing capacity of commercial non-volatile memory cards, this approach is increasingly allowing large numbers of neurons to be continuously recorded wide-band with only a daily battery recharge. The length of our multi-neuron datasets proved particularly advantageous in this study. For example, the theta bursts that we found to be associated with sequential firing were observed very rarely and comprised only 0.1-0.2% of the total duration of each recording. Such events might easily be missed in shorter datasets. In future, the number of channels that can be monitored simultaneously may be increased (theoretically by several orders of magnitude) by incorporating spike sorting to compress the data before storage (Luan et al., 2018). It is to be hoped that these technologies will provide an unprecedented window into how coordinated firing within distributed neural networks during waking and sleeping

607

608 **References**

609 ACHERMANN, P. & BORBELY, A. A. 1997. Low-frequency (< 1 Hz) oscillations in the human sleep
610 electroencephalogram. *Neuroscience,* 81**,** 213-22.
611 BAKER, S. N. & LEMON, R. N. 2000. Precise spatiotemporal repeating patterns in monkey primary
612 and supplementary motor areas occur at chance levels. *J Neurophysiol,* 84**,** 1770-80.
613 BAKER, S. N., SPINKS, R., JACKSON, A. & LEMON, R. N. 2001. Synchronization in monkey motor cortex
614 during a precision grip task. I. Task-dependent modulation in single-unit synchrony. *J*
615 *Neurophysiol,* 85**,** 869-85.
616 BERRY, R. B., BROOKS, R., GAMALDO, C. E., HARDING, S. M., LLOYD, R. M., MARCUS, C. L. & VAUGHN,
617 B. 2015. The AASM Manual for the Scoring of Sleep and Associated Events. *In:* MEDICINE, A.
618 A. O. S. (ed.). Darien, IL, USA.
619 BROOKS, P. L. & PEEVER, J. H. 2012. Identification of the transmitter and receptor mechanisms
620 responsible for REM sleep paralysis. *J Neurosci,* 32**,** 9785-95.
621 BUSH, D., BISBY, J. A., BIRD, C. M., GOLLWITZER, S., RODIONOV, R., DIEHL, B., MCEVOY, A. W.,
622 WALKER, M. C. & BURGESS, N. 2017. Human hippocampal theta power indicates movement
623 onset and distance travelled. *Proc Natl Acad Sci U S A,* 114**,** 12297-12302.
624 BUZSAKI, G. 2002. Theta oscillations in the hippocampus. *Neuron,* 33**,** 325-40.
625 CAMPBELL, S. S. & TOBLER, I. 1984. Animal sleep: a review of sleep duration across phylogeny.
626 *Neurosci Biobehav Rev,* 8**,** 269-300.
627 CANTERO, J. L., ATIENZA, M., STICKGOLD, R., KAHANA, M. J., MADSEN, J. R. & KOCSIS, B. 2003. Sleep-
628 dependent theta oscillations in the human hippocampus and neocortex. *J Neurosci,* 23**,**
629 10897-903.
630 CHURCHLAND, M. M., CUNNINGHAM, J. P., KAUFMAN, M. T., FOSTER, J. D., NUYUJUKIAN, P., RYU, S.
631 I. & SHENOY, K. V. 2012. Neural population dynamics during reaching. *Nature,* 487**,** 51-6.
632 COLGIN, L. L. 2013. Mechanisms and functions of theta rhythms. *Annu Rev Neurosci,* 36**,** 295-312.
633 DESTEXHE, A., CONTRERAS, D. & STERIADE, M. 1999. Spatiotemporal analysis of local field potentials
634 and unit discharges in cat cerebral cortex during natural wake and sleep states. *J Neurosci,*
635 19**,** 4595-608.
636 EUSTON, D. R., TATSUNO, M. & MCNAUGHTON, B. L. 2007. Fast-forward playback of recent memory
637 sequences in prefrontal cortex during sleep. *Science,* 318**,** 1147-50.
638 GOTTESMANN, C. 1992. Detection of seven sleep-waking stages in the rat. *Neurosci Biobehav Rev,*
639 16**,** 31-8.
640 GUPTA, A. S., VAN DER MEER, M. A., TOURETZKY, D. S. & REDISH, A. D. 2012. Segmentation of spatial
641 experience by hippocampal theta sequences. *Nat Neurosci,* 15**,** 1032-9.
642 HALL, T. M., DE CARVALHO, F. & JACKSON, A. 2014a. A common structure underlies low-frequency
643 cortical dynamics in movement, sleep, and sedation. *Neuron,* 83**,** 1185-99.
644 HALL, T. M., NAZARPOUR, K. & JACKSON, A. 2014b. Real-time estimation and biofeedback of single-
645 neuron firing rates using local field potentials. *Nat Commun,* 5**,** 5462.
646 HEADLEY, D. B. & PARÉ, D. 2017. Common oscillatory mechanisms across multiple memory systems.
647 *npj Science of Learning,* 2**,** 1.
648 HOFFMAN, K. L. & MCNAUGHTON, B. L. 2002. Coordinated reactivation of distributed memory traces
649 in primate neocortex. *Science,* 297**,** 2070-3.
650 IBER, C., ANCOLI-ISRAEL, S., CHESSON, A. & QUAN, S. 2007. The AASM Manual for the Scoring of
651 Sleep and Associated Events. *In:* MEDICINE, A. A. O. S. (ed.). Westchester, IL, US.
652 IGARASHI, J., ISOMURA, Y., ARAI, K., HARUKUNI, R. & FUKAI, T. 2013. A theta-gamma oscillation code
653 for neuronal coordination during motor behavior. *J Neurosci,* 33**,** 18515-30.

654 JACKSON, A. & FETZ, E. E. 2007. Compact movable microwire array for long-term chronic unit
655 recording in cerebral cortex of primates. *J Neurophysiol,* 98**,** 3109-18.
656 JACKSON, A., GEE, V. J., BAKER, S. N. & LEMON, R. N. 2003. Synchrony between neurons with similar
657 muscle fields in monkey motor cortex. *Neuron,* 38**,** 115-25.
658 JACKSON, A., MAVOORI, J. & FETZ, E. E. 2006. Long-term motor cortex plasticity induced by an
659 electronic neural implant. *Nature,* 444**,** 56-60.
660 JACKSON, A., MAVOORI, J. & FETZ, E. E. 2007. Correlations between the same motor cortex cells and
661 arm muscles during a trained task, free behavior, and natural sleep in the macaque monkey.
662 *J Neurophysiol,* 97**,** 360-74.
663 JONES, M. W. & WILSON, M. A. 2005. Theta rhythms coordinate hippocampal-prefrontal interactions
664 in a spatial memory task. *PLoS Biol,* 3**,** e402.
665 KAHANA, M. J., SEKULER, R., CAPLAN, J. B., KIRSCHEN, M. & MADSEN, J. R. 1999. Human theta
666 oscillations exhibit task dependence during virtual maze navigation. *Nature,* 399**,** 781-4.
667 KLEINLOGEL, H. 1990. Analysis of the vigilance stages in the rat by fast Fourier transformation.
668 *Neuropsychobiology,* 23**,** 197-204.
669 KRUSKAL, P. B., LI, L. & MACLEAN, J. N. 2013. Circuit reactivation dynamically regulates synaptic
670 plasticity in neocortex. *Nat Commun,* 4**,** 2574.
671 LOUIE, K. & WILSON, M. A. 2001. Temporally structured replay of awake hippocampal ensemble
672 activity during rapid eye movement sleep. *Neuron,* 29**,** 145-56.
673 LUAN, S., WILLIAMS, I., MASLIK, M., LIU, Y., DE CARVALHO, F., JACKSON, A., QUIROGA, R. Q. &
674 CONSTANDINOU, T. G. 2018. Compact standalone platform for neural recording with real-
675 time spike sorting and data logging. *J Neural Eng,* 15**,** 046014.
676 LUCZAK, A., BARTHO, P. & HARRIS, K. D. 2009. Spontaneous events outline the realm of possible
677 sensory responses in neocortical populations. *Neuron,* 62**,** 413-25.
678 MAVOORI, J., JACKSON, A., DIORIO, C. & FETZ, E. 2005. An autonomous implantable computer for
679 neural recording and stimulation in unrestrained primates. *J Neurosci Methods,* 148**,** 71-7.
680 NITSCHE, M. A., JAKOUBKOVA, M., THIRUGNANASAMBANDAM, N., SCHMALFUSS, L., HULLEMANN,
681 S., SONKA, K., PAULUS, W., TRENKWALDER, C. & HAPPE, S. 2010. Contribution of the
682 premotor cortex to consolidation of motor sequence learning in humans during sleep. *J*
683 *Neurophysiol,* 104**,** 2603-14.
684 OKUN, M. 2017. Artefactual origin of biphasic cortical spike-LFP correlation. *J Comput Neurosci,* 42**,**
685 31-35.
686 PENNARTZ, C. M., LEE, E., VERHEUL, J., LIPA, P., BARNES, C. A. & MCNAUGHTON, B. L. 2004. The
687 ventral striatum in off-line processing: ensemble reactivation during sleep and modulation
688 by hippocampal ripples. *J Neurosci,* 24**,** 6446-56.
689 PEYRACHE, A., KHAMASSI, M., BENCHENANE, K., WIENER, S. I. & BATTAGLIA, F. P. 2009. Replay of
690 rule-learning related neural patterns in the prefrontal cortex during sleep. *Nat Neurosci,* 12**,**
691 919-26.
692 PRUT, Y., VAADIA, E., BERGMAN, H., HAALMAN, I., SLOVIN, H. & ABELES, M. 1998. Spatiotemporal
693 structure of cortical activity: properties and behavioral relevance. *J Neurophysiol,* 79**,** 2857-
694 74.
695 RAGHAVACHARI, S., KAHANA, M. J., RIZZUTO, D. S., CAPLAN, J. B., KIRSCHEN, M. P., BOURGEOIS, B.,
696 MADSEN, J. R. & LISMAN, J. E. 2001. Gating of human theta oscillations by a working
697 memory task. *Journal of Neuroscience,* 21**,** 3175-3183.
698 RAMANATHAN, D. S., GULATI, T. & GANGULY, K. 2015. Sleep-Dependent Reactivation of Ensembles
699 in Motor Cortex Promotes Skill Consolidation. *PLoS Biol,* 13**,** e1002263.
700 RUSSO, A. A., BITTNER, S. R., PERKINS, S. M., SEELY, J. S., LONDON, B. M., LARA, A. H., MIRI, A.,
701 MARSHALL, N. J., KOHN, A., JESSELL, T. M., ABBOTT, L. F., CUNNINGHAM, J. P. &
702 CHURCHLAND, M. M. 2018. Motor Cortex Embeds Muscle-like Commands in an Untangled
703 Population Response. *Neuron,* 97**,** 953-966.e8.

SADOWSKI, J. H., JONES, M. W. & MELLOR, J. R. 2016. Sharp-Wave Ripples Orchestrate the Induction of Synaptic Plasticity during Reactivation of Place Cell Firing Patterns in the Hippocampus. *Cell Rep,* 14**,** 1916-29.

SEMBA, K. & KOMISARUK, B. R. 1978. Phase of the theta wave in relation to different limb movements in awake rats. *Electroencephalogr Clin Neurophysiol,* 44**,** 61-71.

STERIADE, M. & MCCARLEY, R. W. 1990. *Brainstem Control of Wakefulness and Sleep,* New York, Springer Science+Business Media.

STERIADE, M., NUNEZ, A. & AMZICA, F. 1993a. Intracellular analysis of relations between the slow (< 1 Hz) neocortical oscillation and other sleep rhythms of the electroencephalogram. *J Neurosci,* 13**,** 3266-83.

STERIADE, M., NUNEZ, A. & AMZICA, F. 1993b. A novel slow (< 1 Hz) oscillation of neocortical neurons in vivo: depolarizing and hyperpolarizing components. *J Neurosci,* 13**,** 3252-65.

STERIADE, M., TIMOFEEV, I. & GRENIER, F. 2001. Natural waking and sleep states: a view from inside neocortical neurons. *J Neurophysiol,* 85**,** 1969-85.

TEO, J. T., SWAYNE, O. B., CHEERAN, B., GREENWOOD, R. J. & ROTHWELL, J. C. 2011. Human theta burst stimulation enhances subsequent motor learning and increases performance variability. *Cereb Cortex,* 21**,** 1627-38.

TUCKER, M. A., MORRIS, C. J., MORGAN, A., YANG, J., MYERS, S., PIERCE, J. G., STICKGOLD, R. & SCHEER, F. 2017. The Relative Impact of Sleep and Circadian Drive on Motor Skill Acquisition and Memory Consolidation. *Sleep,* 40.

VIJAYAN, S., LEPAGE, K. Q., KOPELL, N. J. & CASH, S. S. 2017. Frontal beta-theta network during REM sleep. *Elife,* 25**,** 18894.

VYAZOVSKIY, V. V., RIEDNER, B. A., CIRELLI, C. & TONONI, G. 2007. Sleep homeostasis and cortical synchronization: II. A local field potential study of sleep slow waves in the rat. *Sleep,* 30**,** 1631-42.

WALKER, M. P., BRAKEFIELD, T., MORGAN, A., HOBSON, J. A. & STICKGOLD, R. 2002. Practice with sleep makes perfect: sleep-dependent motor skill learning. *Neuron,* 35**,** 205-11.

WILSON, M. A. & MCNAUGHTON, B. L. 1994. Reactivation of hippocampal ensemble memories during sleep. *Science,* 265**,** 676-9.

YIN, M., BORTON, D. A., KOMAR, J., AGHA, N., LU, Y., LI, H., LAURENS, J., LANG, Y., LI, Q., BULL, C., LARSON, L., ROSLER, D., BEZARD, E., COURTINE, G. & NURMIKKO, A. V. 2014. Wireless neurosensor for full-spectrum electrophysiology recordings during free behavior. *Neuron,* 84**,** 1170-82.

ZANOS, S., RICHARDSON, A. G., SHUPE, L., MILES, F. P. & FETZ, E. E. 2011. The Neurochip-2: an autonomous head-fixed computer for recording and stimulating in freely behaving monkeys. *IEEE Trans Neural Syst Rehabil Eng,* 19**,** 427-35.

Figures legends

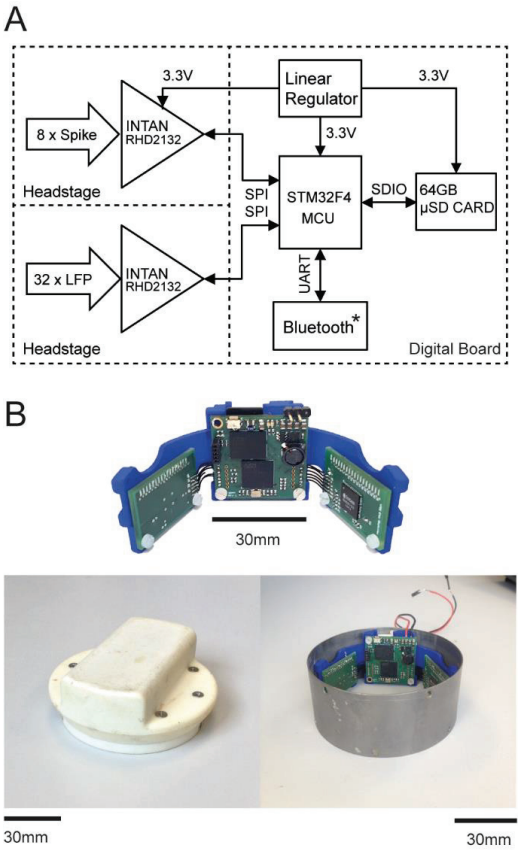

Figure 1. Wearable neural data logger. **A.** System schematic showing main components including two RHD2132 amplifiers (INTAN Technologies, CA, US) amplifiers connecting via a serial peripheral interface (SPI) to a STM43F4 microcontroller unit (MCU, STMicroelectronics, Geneva, Switzerland). **B.** *Top:* Neural data logger PCBs fixed to the support cradle. *Bottom right:* The device fitted inside a titanium headpiece similar to the one used in the monkeys. *Bottom left:* The lid holds the battery and protects the electronics and connectors. The total weight of the electronics plus battery is 152 g.

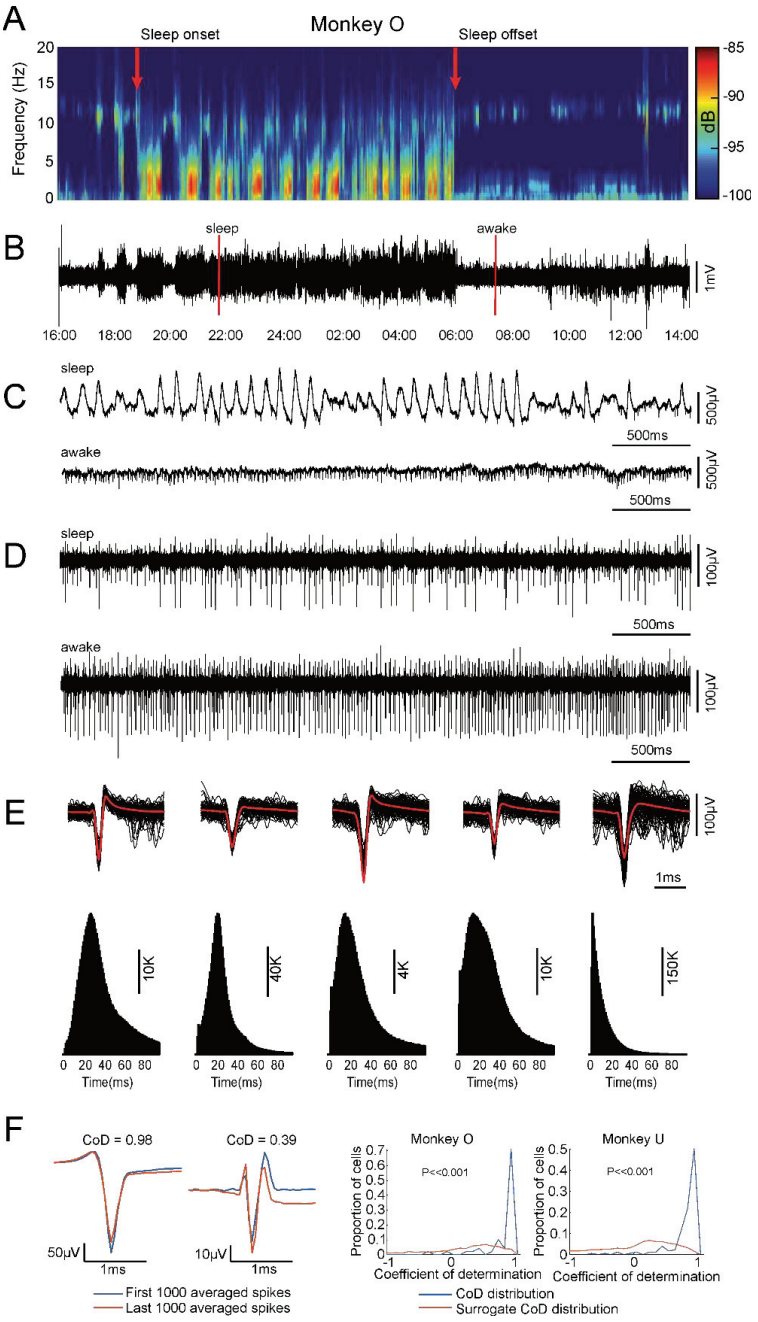

Figure 2. Example motor cortex spike and LFP signals for a typical overnight recording. A. Time-frequency spectrogram of LFP from a single cortical electrode. **B.** LFP waveform for the entire recording period. **C.** 4s windows showing LFP during sleep (*top trace*) and awake (*lower trace*) periods. The two time-points corresponding to these traces are indicated with red lines in panel B. **D.** The same LFP sections as in panel B, after band-

761 pass filtering (1 kHz – 8 kHz) to show action potentials. **E.** Inter-spike interval (ISI)
762 histograms (1 ms bin width) and action potential waveforms for four single-units and one
763 multi-unit spike trains discriminated in a single dataset. **F.** *Left*: average waveform of the first
764 and last 1000 spikes for two example sessions. Waveform stability is indicated by high
765 Coefficients of Determination (CoDs). *Right*: histogram of CoD for all cells (blue trace). Also
766 shown is the surrogate distribution generated by comparing waveform similarity of different
767 neurons in the recording (red trace).
768

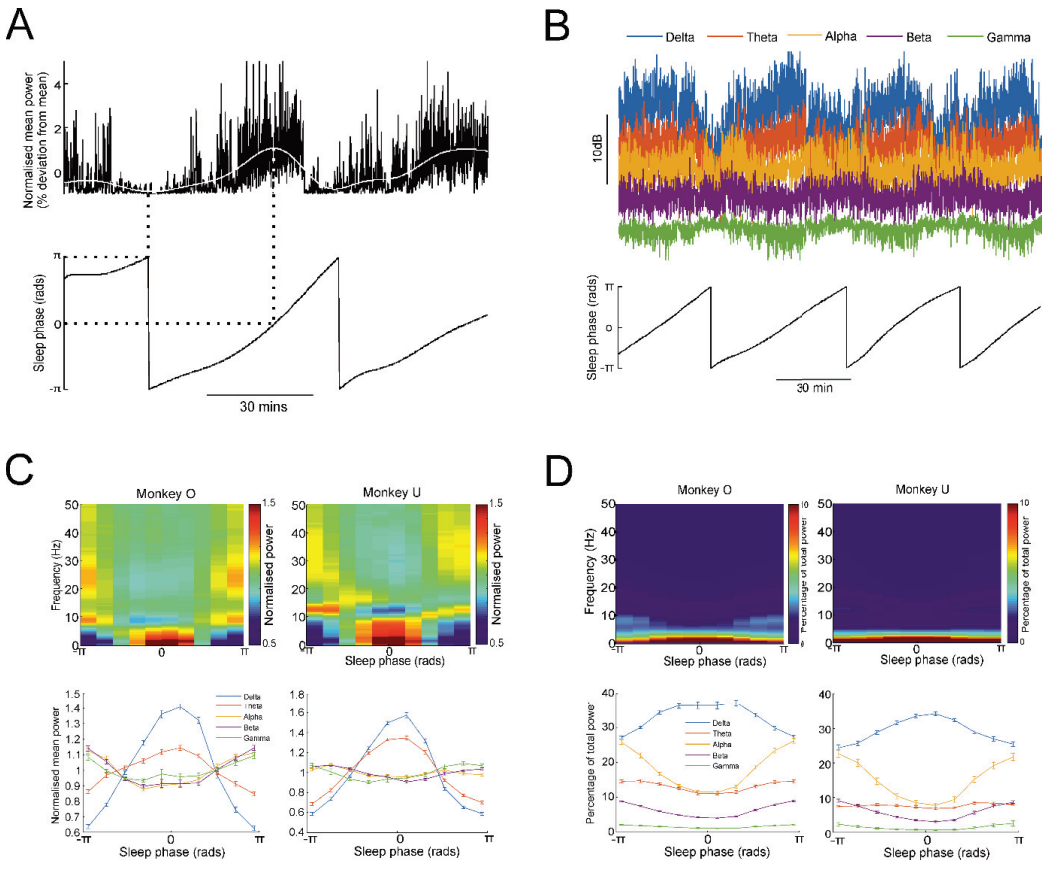

769

770 **Figure 3. LFP power modulation through the sleep cycle. A.** LFP power below 1Hz (*top*,
771 black line) was smoothed (*top*, white line) and used to derive the instantaneous phase of
772 sleep via a Hilbert transform (*bottom*). **B.** LFP power in different frequency bands and
773 associated sleep phase. **C.** LFP power averaged through the sleep cycle (normalized as a

774 proportion of the mean power across the sleep cycle at that frequency). D. LFP power
775 averaged through the sleep cycle (normalized as a proportion of the mean power across all
776 frequencies for that sleep phase).

777

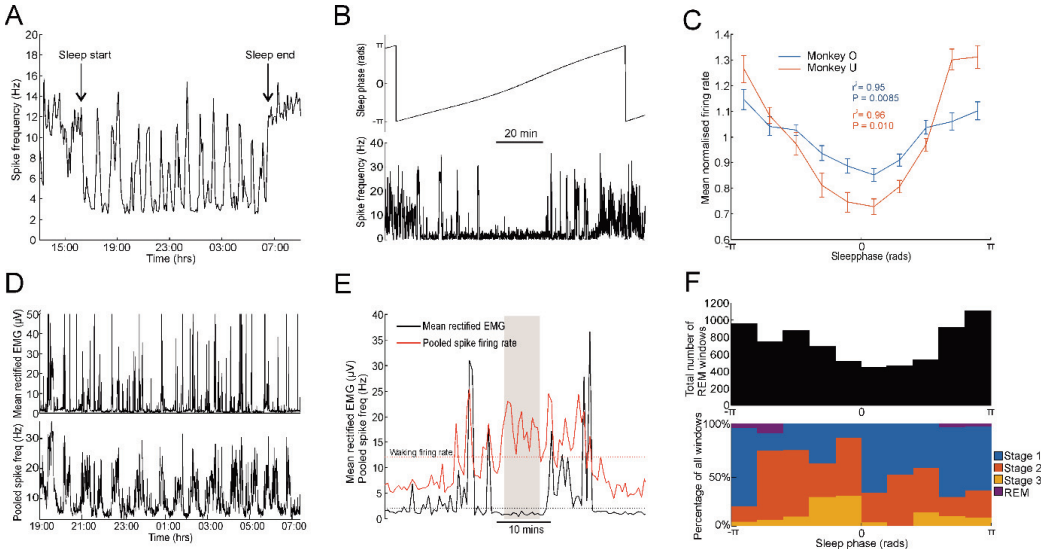

778

779 **Figure 4. Motor cortex firing rates during sleep. A.** Mean firing rate for an example
780 neuron across the duration of an entire recording (divided into 5 minute windows) showing
781 periodic firing rate fluctuations during sleep. **B.** Firing rate (calculated over 2 s windows) for
782 the same cell across a single sleep cycle. **C.** Mean normalized (relative to mean rate) firing
783 for all cells and all sessions. A significant modulation with sleep cycle is demonstrated using
784 circular-to-linear correlation. **D.** Firing of an example neuron together with simultaneously
785 recorded EMG during the night. **E.** Example of period of putative REM sleep (indicated by
786 shading) where spike firing is at frequencies higher than mean waking rates but not
787 associated with muscle activity. **F.** *Top:* Histogram of the instantaneous sleep phases
788 corresponding to all putative REM windows. *Bottom:* Results of manually sleep-scoring
789 sample windows taken from different sleep phases.

790

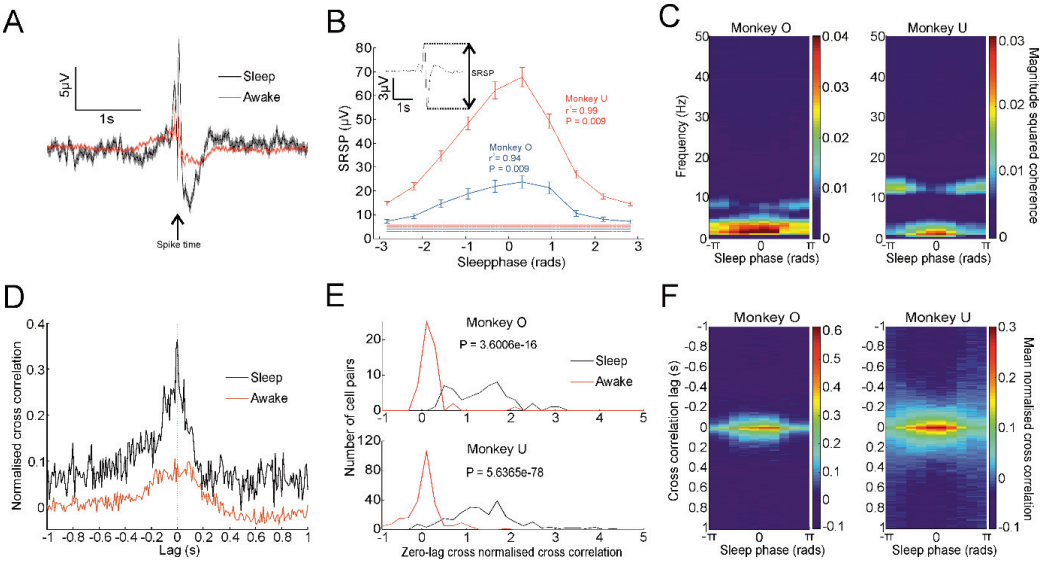

791

792 **Figure 5. Spike-LFP and spike-spike correlations during wake and sleep. A.** Spike
793 triggered average of an LFP showing a similar profile but increased magnitude during sleep
794 vs. awake periods. Shaded regions represent standard error. **B.** Mean SRSP magnitude
795 against sleep phase for all cell and all sessions for both monkeys. Horizontal lines represent
796 mean±SEM of magnitudes during waking. r and P values derived from circular-to-linear
797 correlation analysis. **C.** Mean magnitude squared coherence between spikes and LFPs for
798 frequencies up to 50Hz as a function of sleep phase. **D.** Normalized cross-correlation
799 histogram for an example cell pair during all wake (red line) and sleep (black line) periods of
800 the recording. **E.** Strength of zero-lag correlations between all cell pairs during wake and
801 sleep. **F.** Mean normalized cross-correlation histogram as a function of sleep phase.

802

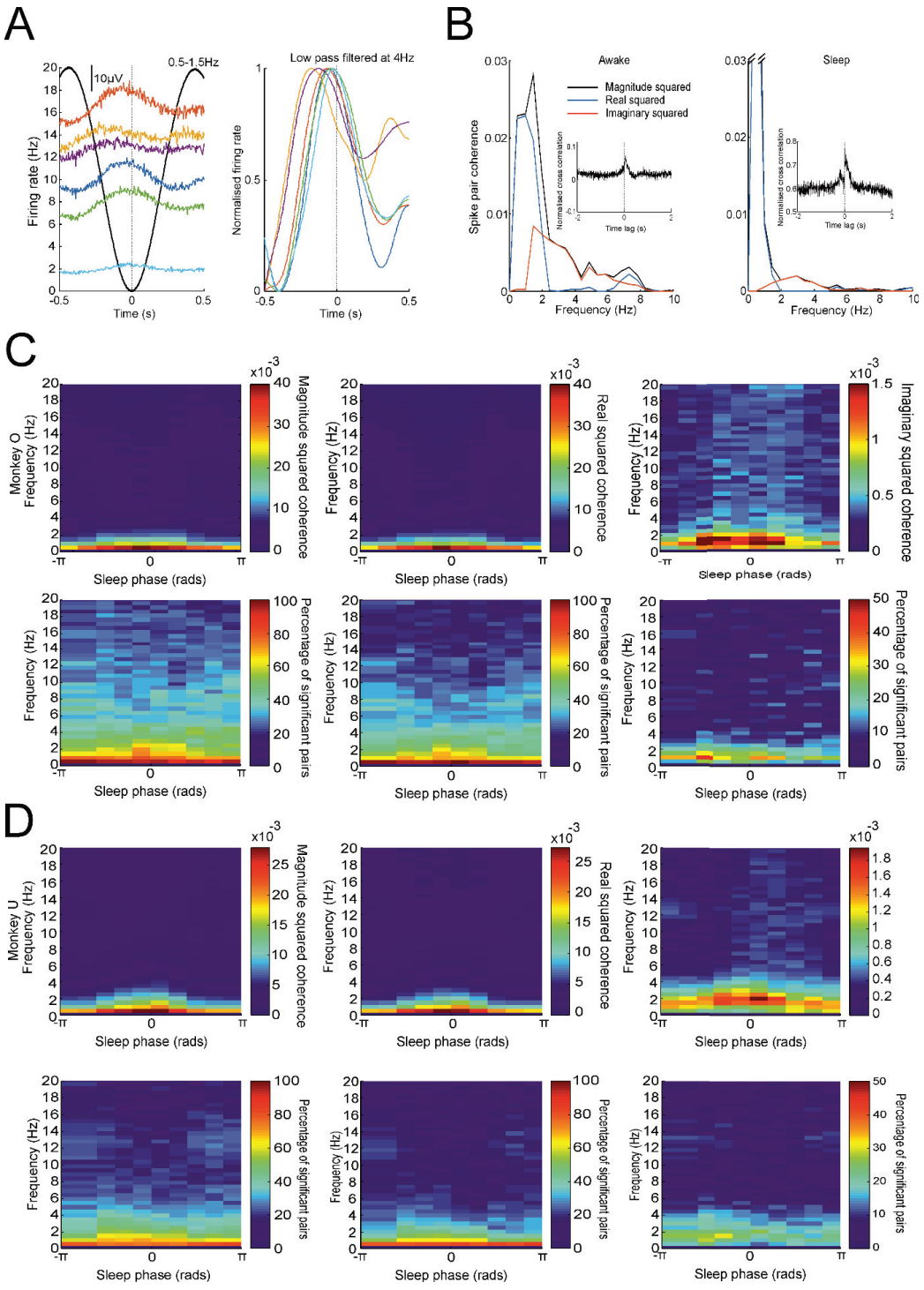

803

804 **Figure 6. Real and imaginary coherence between cell pairs. A.** Average raw (*left*) and

805 filtered/normalized (*right*) spike firing frequency aligned to the trough of low-frequency LFP

for six neurons recorded in a single session. **B.** Magnitude squared, real squared and imaginary squared coherence for an example pair of neurons during sleep (*left*) and waking (*right*). **C, D.** *Top row:* Total, real and imaginary squared coherence for all cell pairs averaged across the sleep cycle for both monkeys. *Bottom row:* proportion of cells pairs exhibiting significant (P<0.05) coherence at each frequency across the sleep cycle.

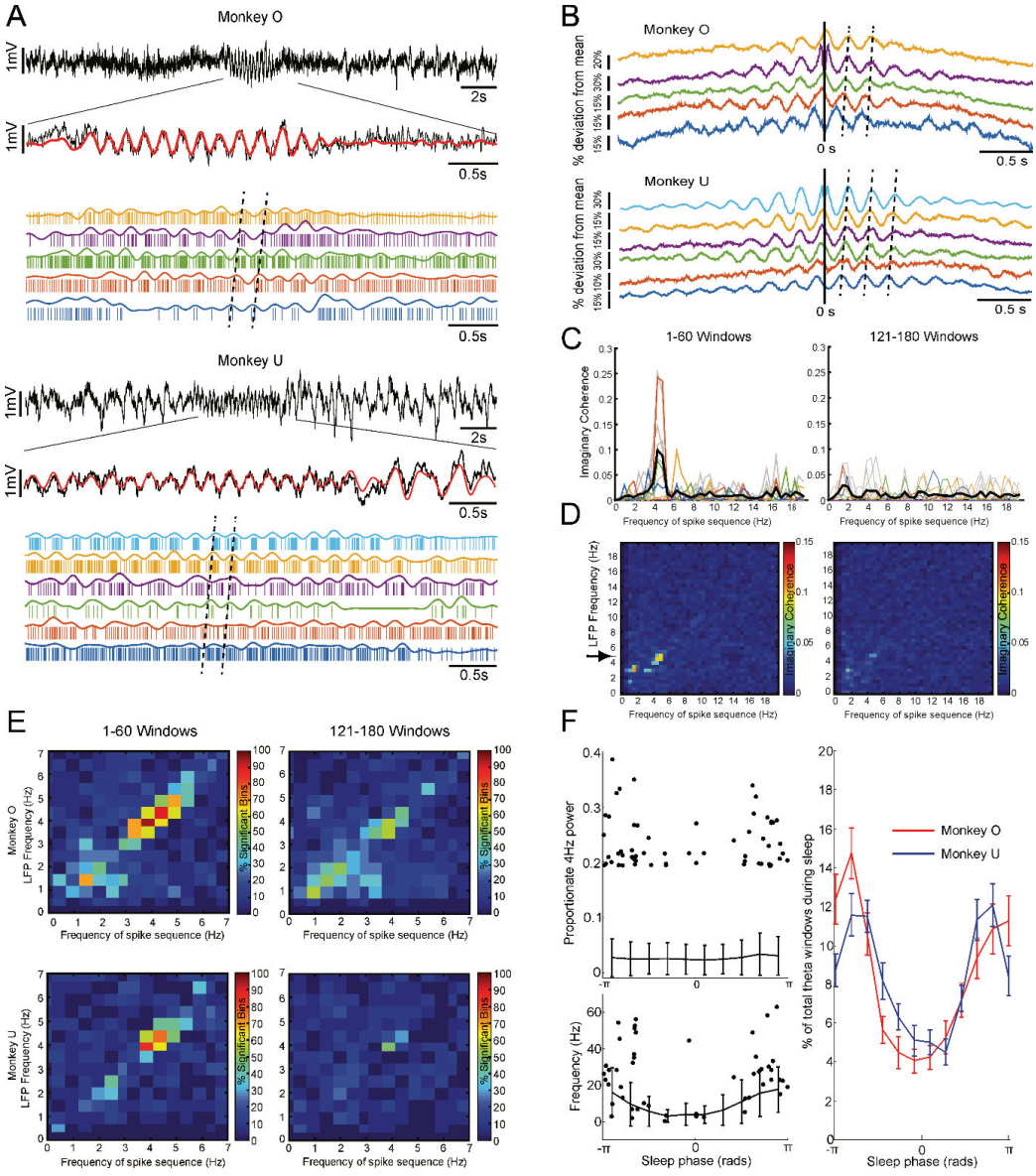

Figure 7. Sequential firing during theta bursts. A. Examples of LFP theta bursts with corresponding neural spiking shown in the expanded traces below. Note that different neurons are plotted in order of firing during the theta cycle. **B.** Example cross-correlation histograms during periods of high LFP theta. Cross-correlations for all cells relative to a single reference cell are shown. **C.** Imaginary coherence between spike trains during the top 60 windows of highest LFP theta (*left*). Colored lines correspond to the cross-correlation histograms shown above (Monkey O), while grey lines show all other cell pairs in this recording. The black trace shows the average over cell pairs. Also shown (*right*) is the corresponding analysis applied to windows ranked 121^{st} – 180^{th} in LFP theta. **D.** Mean imaginary coherence for the same session computed over windows sorted according to a range of LFP frequencies (0 Hz – 20 Hz). **E.** Proportion of all datasets exhibiting significant imaginary coherence at each firing rate frequency, when calculated over windows sorted according to all LFP frequencies. Significant sequential firing at theta frequencies is a consistent finding, but only for windows exhibiting high LFP theta. **F.** *Left*: Solid lines indicate mean theta power and mean spike firing rate as a function of sleep and high power theta power. Error bars represent standard deviation. Dots indicate theta power and firing rate associated with the top 60 windows of highest LFP theta for an example session in Monkey U. *Right*: sleep phase associated with the top 60 windows of highest LFP theta over all sessions.

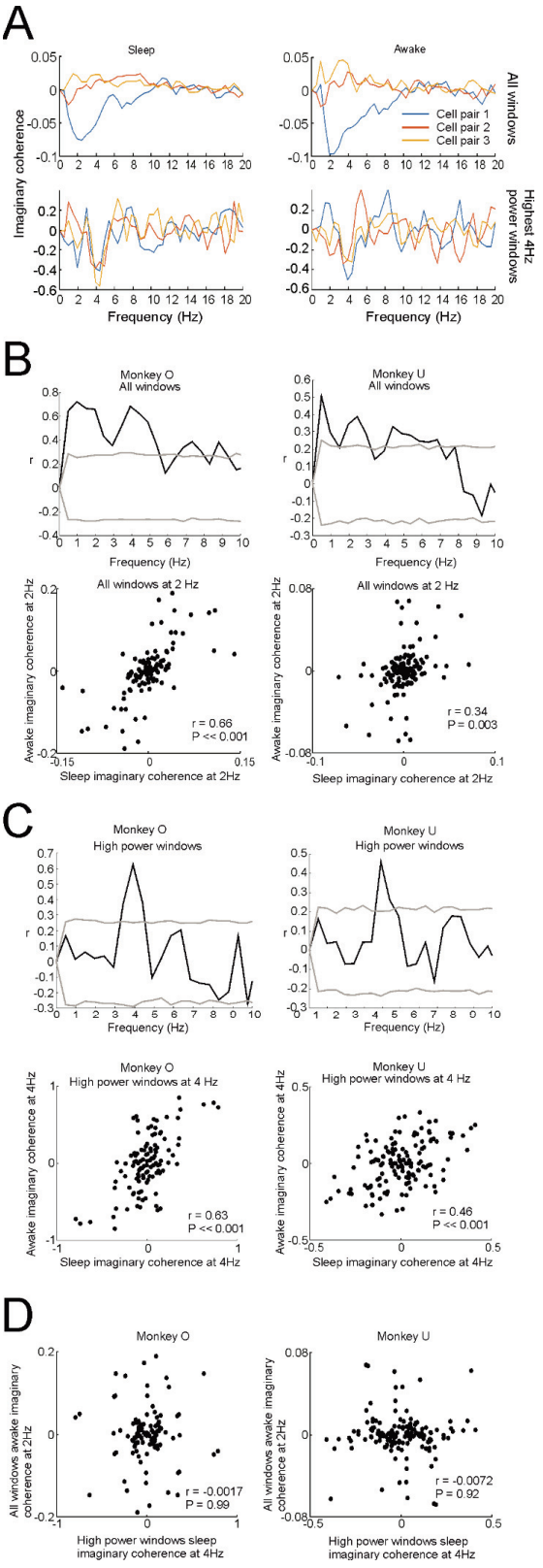

833

834 **Figure 8. Consistent sequential firing between sleep and waking. A.** Signed imaginary
835 coherence spectra for 3 example neuron pairs during sleep (*left*) and waking (*right*) periods,
836 calculated for all windows (*top*) and during theta bursts (*bottom*). **B.** *Top row:* correlation
837 coefficient between pairwise imaginary coherence values in wake and sleep (all windows),
838 across all neuron pairs for both monkeys. Grey lines indicate 95% significance thresholds
839 obtained by shuffling across neurons. *Bottom row:* scatter plot of sleep vs awake imaginary
840 coherence at an example frequency of 2Hz. **C.** *Top row:* correlation coefficient between
841 pairwise imaginary coherence values in wake and sleep (during theta bursts), across all
842 neuron pairs for both monkeys. Grey lines indicate 95% significance thresholds obtained by
843 shuffling across neurons. *Bottom row:* scatter plot of sleep vs awake imaginary coherence at
844 an example frequency of 4Hz. **D.** Scatter plot of imaginary coherence values at 4Hz (during
845 theta bursts) against imaginary coherence at 2 Hz (during all waking periods).
846

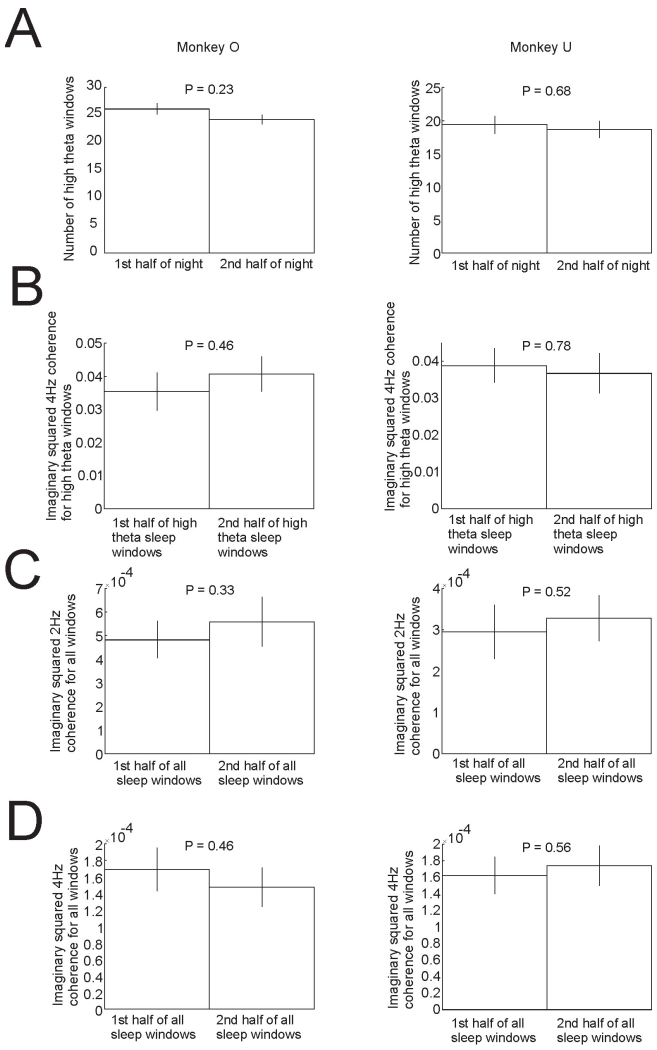

Figure 9. No evidence for change in theta and delta sequence strength during sleep. A. Number of high power theta windows in first and second half of sleep. B. Mean theta imaginary squared coherence values during theta bursts in the first and second half of sleep. C. Mean delta imaginary squared coherence values in the first and second half of all windows during sleep. D. Mean theta imaginary squared coherence values in the first and second half of all windows during sleep. (P values from paired t-test).

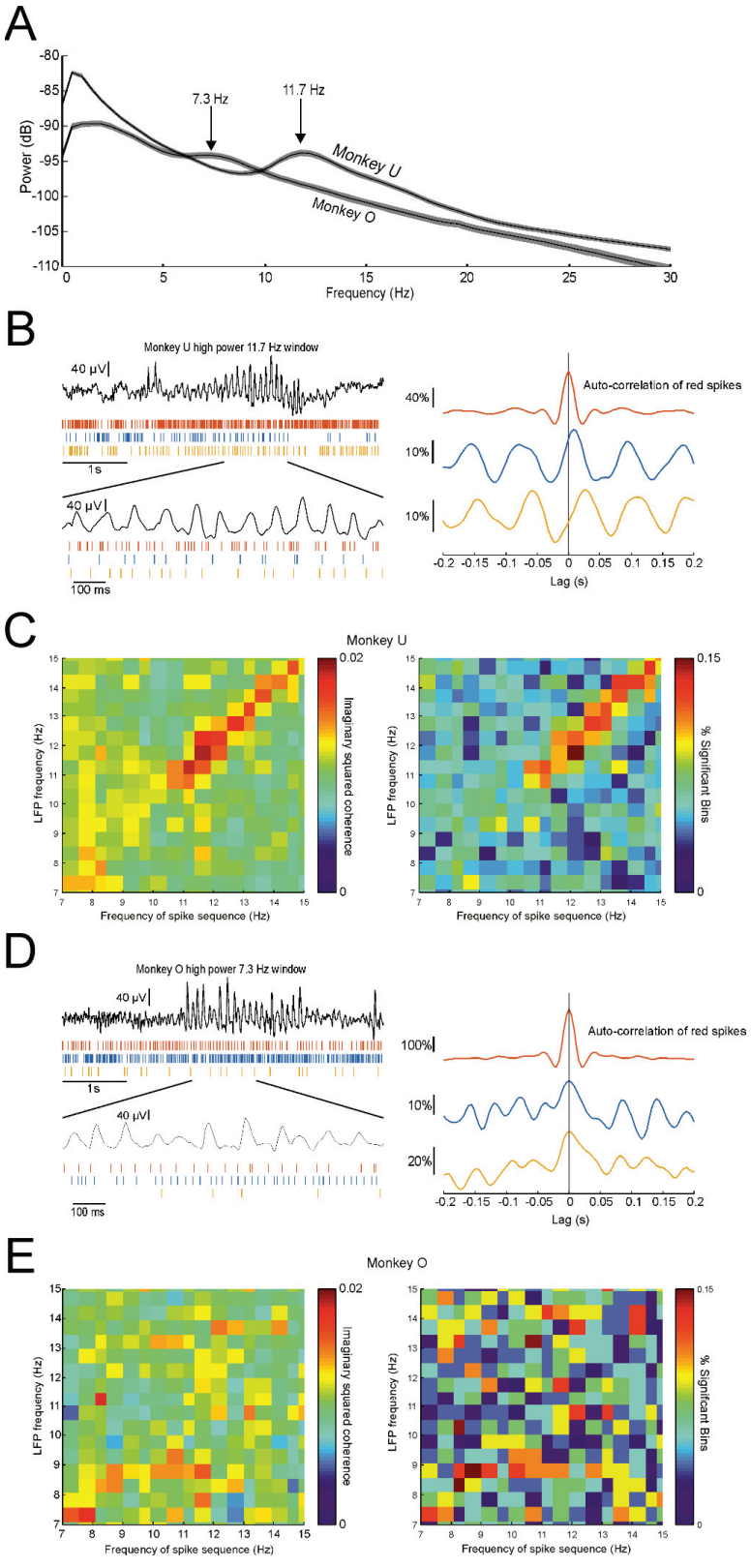

857

Figure 10. Inconsistent sequential firing during high power alpha windows. A. Averaged power spectrum of all LFPs in both monkeys during sleep showing peaks at different frequencies in the alpha/sigma frequency range. B. *Left*: example LFP from monkey U showing putative sleep spindle and concurrent spikes from three neurons. *Right*: example cross-correlation histogram showing sequential firing during spindles. C. *Left*: mean imaginary squared coherence for all spike pairs during 60 windows with highest relative power at frequencies from 7 to 20Hz during sleep for monkey U. *Right*: proportion of sessions exhibiting significant imaginary coherence for monkey U. D. *Left*: LFP segment from monkey O showing putative sleep spindle and concurrent spike firing. *Right*: example cross-correlation histogram showing only synchronous firing during spindles. E. *Left*: mean imaginary squared coherence for all spike pairs during highest 60 windows with highest relative power at frequencies from 7 to 20Hz during sleep for monkey O *Right*: proportion of sessions exhibiting significant imaginary coherence for monkey O.

A

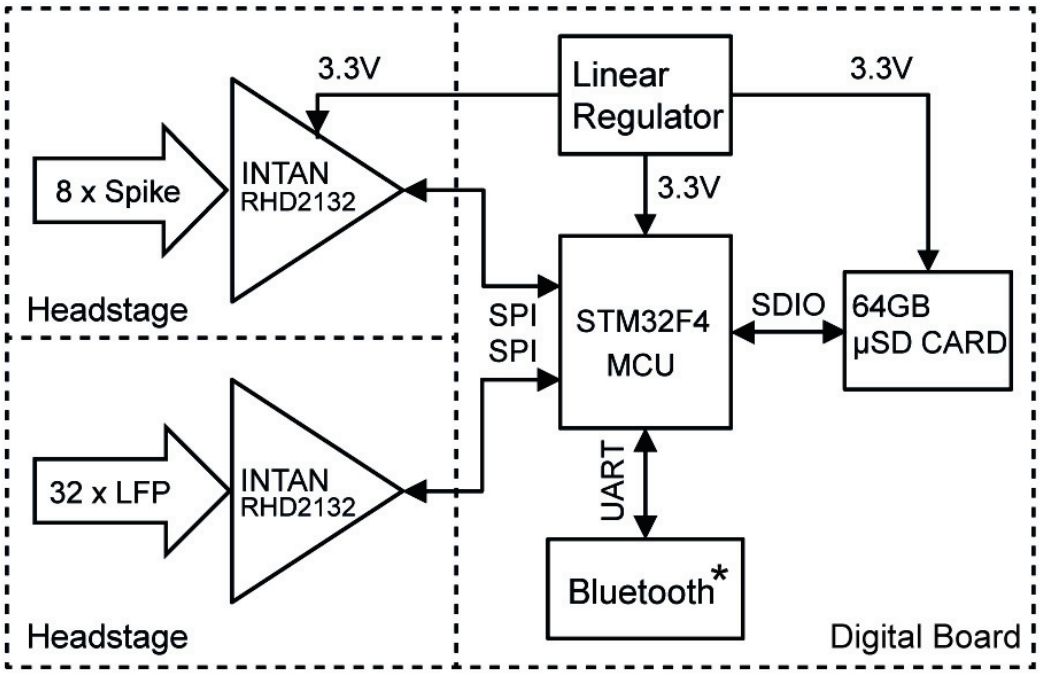

B

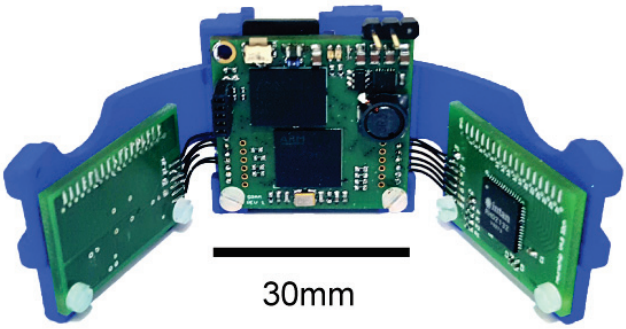

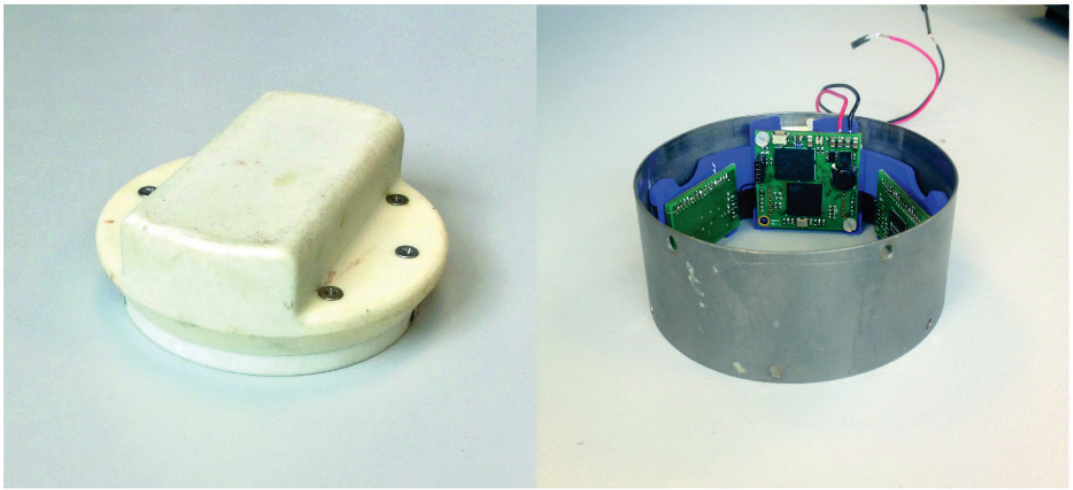

30mm

30mm